J. Fluid Mech. (1988), *vol.* 195, *pp.* 281–302
Printed in Great Britain

Steep, steady surface waves on water of finite depth with constant vorticity

By A. F. TELES DA SILVA† AND D. H. PEREGRINE
School of Mathematics, Bristol University, University Walk, Bristol BS8 1TW, UK

(Received 21 December 1987)

Two-dimensional steady surface waves on a shearing flow are computed for the special case where the flow has uniform vorticity, i.e. in the absence of waves the velocity varies linearly with height. A boundary-integral method is used in the computation which is similar to that of Simmen & Saffman (1985) who describe such waves on deep water. Particular attention is given to the effects of finite depth with descriptions of waves of limiting steepness, waves with eddies beneath their crests and extremely high waves on high-speed flows.

Many qualitative features of these waves are relevant to steep waves propagating in shallow water, or on a strong wind-induced drift current. An important practical point in the interpretation of wave measurements of wind driven waves is that mean kinetic energy and potential energy densities are unequal even for infinitesimal waves. This may mean that wave energy spectra deduced from surface-elevation measurements in the conventional way may sometimes be misleading.

1. Introduction

Most of the theoretical results concerning surface waves on water make the initial assumption of irrotational flow. There are many circumstances in which this is well justified. However there are cases where it is inappropriate. Two examples are particularly common and can serve to orient discussion. Waves are most commonly generated by wind and in any region where the wind is blowing there is a surface drift of the water. Banner & Phillips (1974) demonstrate that a thin wind-drift boundary layer can have $O(1)$ effects on the maximum height of a steady gravity wave. They simply consider Bernoulli's equation in a reference frame moving with the wave. Theoretical studies of the initial instability of wind over water include the velocity shear and have recently been well supported by experimental evidence (Caulliez 1987).

Currents always cause shear at the bed of the sea or of a river. If the water is shallow and waves are long the shear can become a dominant feature in the waves' dynamics. Peregrine (1974) described very steep waves arising when there is strong shear near the water surface and modelled them by considering a thin jet of water flowing at the surface.

Theoretical work on waves propagating on currents that vary with depth is reviewed in Peregrine (1976, §4). Results for steep waves can be divided into two classes: (i) weakly nonlinear waves obtained by a perturbation expansion and (ii) numerical solutions mainly for constant vorticity. Of the works on weakly nonlinear waves two merit particular mention. Tsao (1959) studies waves with constant vorticity and water depth with a third-order Stokes expansion. Benjamin (1962)

† On leave from Instituto de Matemática da UFRJ, Ilha do Fundão, Rio de Janeiro RJ, Brazil.

recasts the problem into an equation for streamline height and finds solitary-wave solutions. Numerical work has been largely for constant vorticity; Dalrymple (1974) takes two layers of constant vorticity with finite water depth and uses a Fourier series expansion of the stream function, and Simmen & Saffman (1985) solve for very steep waves in deep water by discretizing a boundary-integral expression.

The present work is confined to two-dimensional inviscid steady waves with constant vorticity. An inviscid approximation is often realistic since the velocity profile in the water, whether due to laminar viscosity or turbulent mixing, is usually established over timescales and lengthscales which are long compared with a wave period or wavelength. Emphasis is given to steep waves and the effects of finite depth.

The choice of constant vorticity simplifies the mathematics considerably. Whether or not important aspects of the flow are lost when compared with a more realistic vorticity distribution is less clear. For two cases it is likely that the constant vorticity solutions are representative. One is when waves are short compared with the lengthscale of the vorticity distribution; then they are deep water waves and are sufficiently short that they are only influenced by the value of vorticity at the surface. Since Simmen & Saffman (1985) deal with deep-water waves, this case is not discussed here in detail. The other case where constant vorticity may give a good description is when the waves are long compared with the water depth. In this case it is the existence of a non-zero mean vorticity that is important rather than its specific distribution; a matter that is returned to in discussion of the solutions.

In the next two sections the mathematical background and method is described. The numerical method has many similarities to that of Simmen & Saffman (1985).

The parameter space of solutions has three dimensions corresponding to the usual variations with amplitude and wavelength or period plus a variation with vorticity. The whole parameter space is not fully described. Emphasis is given to the solitary-wave limit where variations of wave amplitude and vorticity are considered. The solutions which differ most from irrotational waves are high waves with large Froude numbers. These high waves enclose large regions of closed circulation and are discussed in some detail since their shape appears to be insensitive to the vorticity distribution.

The flows described are idealized and in that respect many details are of academic interest, on the other hand general features of the waves are important for applications. Some of the features such as the variation in steepness of the limiting waves, and the tendencies for waves to become more or less sharply peaked as vorticity varies are relatively well known. We draw particular attention to the considerable differences that can exist between the potential and kinetic energy densities of waves with vorticity. This could be important in studying the energetics of waves in a strong wind. The detailed solutions corresponding to the very large waves which are found on very high Froude number flows could also be valuable since these are likely to form in civil engineering works, e.g. the 'wave' hydraulic jump, and seem to be similar to the waves formed over antidunes in supercritical flow over mobile beds.

2. Mathematical preliminaries and analytic approximations

A steady two-dimensional incompressible flow may be described by a stream function $\Psi(x, y)$, in which case

$$\nabla^2 \Psi = -\zeta, \tag{2.1}$$

where ζ is the vorticity, which is perpendicular to the (x, y)-plane. If vorticity is uniform and constant throughout the flow then Kelvin's circulation theorem can be used to show that it remains constant whilst the flow remains two-dimensional and simply connected. Hence (2.1) holds within the fluid and Ψ can be rewritten as the sum of a particular integral satisfying (1.1) and an irrotational stream function $\psi(x, y)$. It is this feature of constant vorticity flows that simplifies analysis.

We choose a reference frame in which the wave is at rest, $y = 0$ is the undisturbed free surface or mean water level and $y = -h$ is the plane rigid bed. The water velocity $\boldsymbol{u}$ is described by

$$\boldsymbol{u} = (\phi_x - \zeta y - c, \phi_y), \tag{2.2}$$

in which ϕ is a velocity potential for the finite perturbation to a horizontal flow with constant vorticity ζ. The stream function

$$\Psi = -\tfrac{1}{2}\zeta y^2 - cy + \psi(x, y), \tag{2.3}$$

where ψ and ϕ describe the same irrotational perturbation. The constant c represents the wave velocity relative to the 'original' water velocity at the surface.

The definition of the waves' phase velocity is not a trivial matter. We use the equivalent of Stokes's (1847) first definition of velocity, i.e. the perturbation velocity due to the wave at any point below a wave trough is chosen to be such that its phase average is zero, i.e. in this case ϕ and ψ are periodic functions of x. Stokes's second definition of phase velocity is the wave speed which gives zero mass flow. For a linearized wave in this case, this alternative definition gives

$$c_2 = c - \tfrac{1}{2}\zeta h, \tag{2.4}$$

whereas for linearized irrotational waves the velocities would be identical.

The stream function ψ and velocity potential ϕ both satisfy Laplace's equation within the fluid.

The kinematic boundary conditions are

$$\Psi = -\tfrac{1}{2}\zeta y^2 - cy + \psi = \text{constant}, \tag{2.5}$$

at the free surface $y = \eta(x)$, and

$$\phi_y = 0, \tag{2.6}$$

on the bed, $y = -h$. The constant pressure condition at the free surface becomes

$$\tfrac{1}{2}(\phi_x - \zeta y - c)^2 + \tfrac{1}{2}\phi_y^2 + g\eta = B, \tag{2.7}$$

after using Bernoulli's equation.

The linearized solution is readily found and gives a dispersion relation which can be written

$$c_0^2 - \frac{\zeta c_1^2}{g} c_0 - c_1^2 = 0, \tag{2.8}$$

where c_0 is the linear phase velocity and

$$c_1^2 = (g/k)\tanh(kh) \tag{2.9}$$

is the dispersion relation for linearized irrotational waves of wavenumber k. Solving the quadratic (2.8) for c_0 gives

$$c_0 - \zeta\frac{c_1^2}{2g} = \pm c_1\left(1 + \frac{\zeta^2 c_1^2}{4g^2}\right)^{\frac{1}{2}}. \tag{2.10}$$

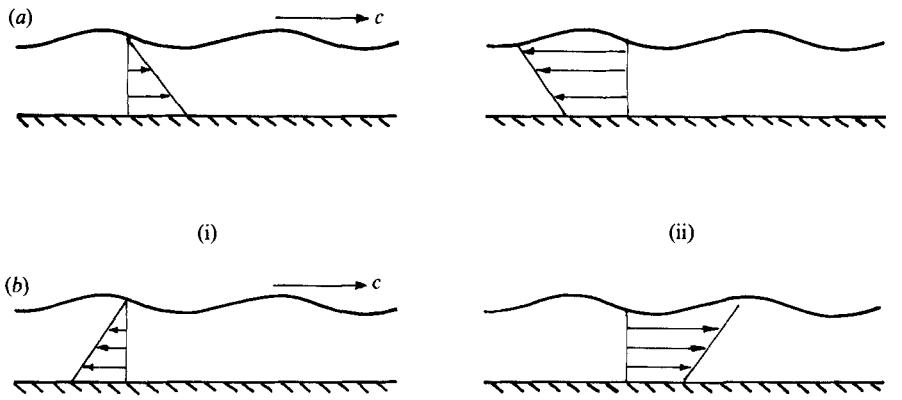

FIGURE 1. Sketches indicating wave direction and shear profile. On the left (i) is the configuration we use, and on the right (ii) the equivalent wave stationary on a stream. (*a*) Wave propagating upstream, positive vorticity. (*b*) Wave propagating downstream, negative vorticity.

Using (2.9) and comparing with the undisturbed flow we can interpret (2.10) as showing that the waves travel symmetrically with respect to the flow at a depth

$$W = \frac{c_1^2}{2g} = \frac{\tanh(kh)}{2k}, \tag{2.11}$$

which gives a measure of the depth of water which influences the wave properties, or 'wave depth'. The limiting values of W for large and small kh are $\frac{1}{2}k^{-1}$ and $\frac{1}{2}h$ respectively. The right-hand side of (2.10) shows that shear increases the wave speed of linearized waves.

A critical layer occurs in the flow if at any depth

$$c = -\zeta y,$$

let $h_c = c/\zeta$ be the critical layer depth. Substitution in the linear dispersion equation (2.8) and use of the wave depth, W, gives

$$h_c = W + W\left(1 + \frac{2g}{\zeta^2 W}\right)^{\frac{1}{2}},$$

for linear waves.

Thus if there is a critical layer it is always at a depth greater than $2W$, and then only near $2W$ for strong shears. Critical layers only occur for waves propagating 'upstream', and when

$$\zeta > \left[\frac{g \tanh kh}{h(kh - \tanh kh)}\right]^{\frac{1}{2}}. \tag{2.12}$$

In order to fix ideas we shall only consider positive values of c and k but allow ζ to have either sign. For convenience of description we shall refer to 'upstream' and 'downstream' in the sense of waves propagating on a flowing stream with maximum velocity at the surface. See figure 1 (*a*) in which our configuration for ζ positive is shown and the effect of a stream giving wave propagation 'upstream'. Similarly figure 1 (*b*) shows ζ negative and the corresponding 'downstream' propagation. The downstream case is equivalent to downwind propagation for the case of a shear generated by the wind.

Tsao (1959) extends the linear theory to a third-order solution following the same type of approach as for the irrotational Stokes-wave expansion. Tsao's results, in particular phase-speed, have been checked and agree† with our computed results.

Tsao's results show that upstream propagating waves are more rounded, i.e. have less deviation from a sinusoidal wave, whilst downstream propagating waves have sharper steeper crests. As in the irrotational Stokes waves successive terms in the expansion increase as depth decreases. They also increase as the vorticity becomes more strongly negative.

3. Numerical method of solution

Units are chosen so that $k = 1$ and $g = 1$. This means that the wavelength is 2π. We work with the complex velocity

$$q(z) = u - \mathrm{i}v = \frac{\mathrm{d}f}{\mathrm{d}z},$$

where $f = \phi + \mathrm{i}\psi$. The boundary condition (2.6) on the bed is satisfied by considering an image region, see figure 2(*a*). The area within one wavelength and its image is mapped from the z-plane, with the transformation

$$Z(z) = \exp(-\mathrm{i}z), \tag{3.1}$$

to give a closed region in the Z-plane, see figure 2(*b*). The complex velocity potential is chosen to be periodic so $f(z)$ transforms to a single-value function $F(Z)$ in the Z-plane, analytic between S and S' (see figure 2 for notation). The complex velocity transforms

$$q(z) = \frac{\mathrm{d}f}{\mathrm{d}z} = -\mathrm{i}Z\frac{\mathrm{d}F}{\mathrm{d}Z} = -\mathrm{i}ZQ(Z). \tag{3.2}$$

For a point on the surface S in the Z-plane Cauchy's integral theorem for a complex function gives

$$Q(Z) = \frac{1}{\pi\mathrm{i}}PV\int_{S+S'}\frac{Q(Z')\,\mathrm{d}Z'}{Z-Z'},$$

and hence from (3.2)

$$\frac{q(z)}{Z(z)} = \frac{1}{\pi\mathrm{i}}PV\int_{BA+A'B'}\frac{q(z')\,\mathrm{d}z'}{Z(z)-Z(z')}. \tag{3.3}$$

Figure 2 shows the curves over which the integrals are taken.

We now introduce a parametrization of the surface of the fluid. Let the surface be

$$R(\xi) = x(\xi) + \mathrm{i}y(\xi). \tag{3.4}$$

The parameter ξ is important in the discretization of the surface which is used in the numerical approximation. It is given integer values at discretization points. The parameterization is also chosen in such a manner that (i) points are concentrated near the crest of a wave where they are usually needed to resolve higher curvatures,

† Equation (2.19) in Tsao (1959) should read, in Tsao's notation:

$$C_2 = \tfrac{1}{2}a^2b(ck + \tfrac{1}{2}b).$$

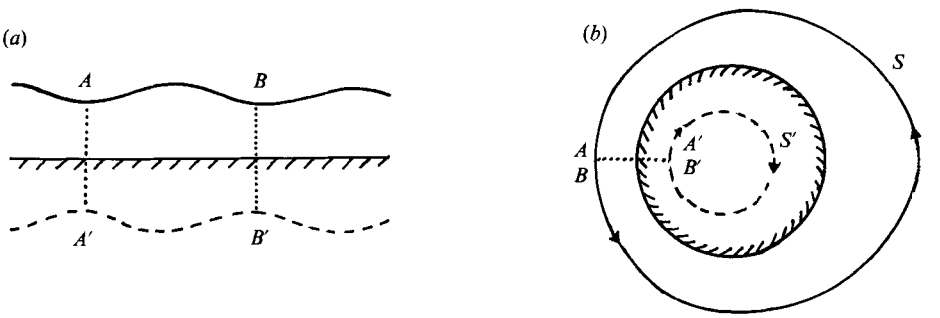

FIGURE 2. (*a*) The region of water beneath one wavelength and its image at the z-plane. (*b*) Transformed region in the Z-plane.

and (ii) $R(\xi)$ is an analytic function of ξ so that high-order numerical approximations can easily be found and used with the equispaced discretization of ξ.

We require the parameterization to satisfy:

$$\frac{\mathrm{d}s}{\mathrm{d}\xi} = \frac{K|q-\zeta y-c|}{1+\alpha \sin^2 \tfrac{1}{2}x}, \tag{3.5}$$

where s is arclength, K is a constant to be determined in the numerical solution and α is given as a parameter. If we take α to be zero we have Simmen & Saffman's (1985) parameterization where $\mathrm{d}s/\mathrm{d}\xi$ decreases as we approach the wave crest, ensuring a concentration of numerical points in that region. As the crest is usually placed at $x = \pi$ we have for positive values of α a still stronger concentration of points near the crest and a consequent rarefaction at the troughs, that proves to be useful when dealing with steep waves (Tanaka 1983, 1985) and with waves in very shallow water. On the other hand big upstream propagating waves tend to have higher curvatures at the troughs and in that case negative values of α can reduce concentration near the crests.

The flat bed is chosen to be at $y = -h$. A point z_2 on $A'B'$ is the image in the bed of a point z_1 on AB where

$$z_2 = z_1^* - 2\mathrm{i}h, \tag{3.6}$$

(the asterisk denotes complex conjugate), thus

$$Z(z_2) = \mathrm{e}^{-2h}\, Z(z_1^*) = \frac{\mathrm{e}^{-2h}}{Z^*(z_1)}, \tag{3.7}$$

and the velocity reflects to give

$$q(z_2) = q^*(z_1). \tag{3.8}$$

In addition waves are presumed to be symmetrical about crests and troughs and reflection about the plane $x = 0$, chosen to be at a trough, gives that an image point z_3 is

$$z_3 = -z_1^*, \tag{3.9}$$

$$Z(z_3) = Z(-z_1^*) = 1/Z(z_1), \tag{3.10}$$

$$q(z_3) = q^*(z_1). \tag{3.11}$$

The effect of the above reflections and introduction of the parameterization is that (3.3) can be rewritten:

$$\frac{\pi q(\xi)}{Z(\xi)} = PV\int_0^n \frac{q(\xi')\,R_\xi(\xi')\,\mathrm{d}\xi'}{Z(\xi)-Z(\xi')} + \int_0^n \left\{ \frac{q^*(\xi')\,R_\xi^*(\xi')}{Z(\xi)-1/Z(\xi')} - \frac{q^*(\xi')\,R_\xi^*(\xi')}{Z(\xi)-\mathrm{e}^{-2h}/Z^*(\xi')} - \frac{q(\xi')\,R_\xi(\xi')}{Z(\xi)-\mathrm{e}^{-2h}/Z(\xi')} \right\} \mathrm{d}\xi', \quad (3.12)$$

where notation is simplified by suppressing dependence on z.

Boundary conditions at the surface are incorporated as follows. The kinematic condition that the velocity is parallel to the surface tangent may be written:

$$|q-\zeta y-c|\,R_s = q^*-\zeta y-c. \quad (3.13)$$

Bernoulli's equation (2.7) at the surface is:

$$|q-\zeta y-c|^2 = 2(B-gy). \quad (3.14)$$

With the relations (3.13) and (3.5) the left-hand side of (3.12) is

$$\pi q(\xi)/Z(\xi) = \pi/Z(\xi)\,[c+\zeta y-(1+\alpha\sin^2\tfrac{1}{2}x)\,R_\xi^*(\xi)/K] = F(\xi) \quad (3.15)$$

say. The expression qR_ξ which occurs in all the integrals on the right-hand side of (3.12) can be written

$$qR_\xi = (\zeta y+c)R_\xi + 2K(B-gy)/(1+\alpha\sin^2\tfrac{1}{2}x) = G(\xi) \quad (3.16)$$

say. With the substitutions of (3.15) and (3.16) in (3.12) it becomes an integro-differential equation for the functions $x(\xi)$ and $y(\xi)$.

To fix the solution we also impose that the height of the wave

$$H = y(n)-y(0), \quad (3.17)$$

and its mean level is at $y = 0$, i.e.

$$\int_A^B y\,\mathrm{d}x = 0. \quad (3.18)$$

The mean velocity of the irrotational perturbation is chosen to be zero, and becomes

$$2K\int_0^n \frac{(B-gy)\,\mathrm{d}\xi}{(1+\alpha\sin^2\tfrac{1}{2}x)} + \pi c = 0 \quad (3.19)$$

after using (3.16).

In order to discretize the integrals for numerical solutions it is necessary to deal with the singular integral in (3.12). Following Dold & Peregrine (1986)

$$\int_0^n \frac{G(\xi')\,\mathrm{d}\xi'}{Z(\xi)-Z(\xi')} = \left(\int_0^{\xi-\frac{1}{2}} + \int_{\xi+\frac{1}{2}}^n\right) \frac{G(\xi')\,\mathrm{d}\xi'}{Z(\xi)-Z(\xi')} + \int_{\xi-\frac{1}{2}}^{\xi+\frac{1}{2}} \left(\frac{G(\xi')}{Z(\xi)-Z(\xi')} - \frac{G(\xi)}{Z_\xi(\xi)\,(\xi-\xi')} \right) \mathrm{d}\xi'. \quad (3.20)$$

The extra term in the last integral makes zero contribution but eliminates the singularity since the whole integrand approaches

$$\frac{G_\xi(\xi)}{Z_\xi(\xi)}+\frac{G(\xi)\,Z_{\xi\xi}(\xi)}{2Z_\xi^2(\xi)} \tag{3.21}$$

as $\xi' \to \xi$.

Discretizing (3.12) by means of a trapezoidal rule, which is the most accurate formula for integrating periodic functions given at equispaced points, using (3.21) and giving integral values to ξ we have the following set of equations

$$\sum_{\substack{\xi'=0\\ \xi'\neq\xi}}^{\xi'=n}\left(\frac{G(\xi')}{Z(\xi)-Z(\xi')}-\frac{G^*(\xi')}{Z(\xi)-\mathrm{e}^{-2h}/Z^*(\xi')}\right)+\frac{G^*(\xi)}{\mathrm{i}R_\xi(\xi)\,Z(\xi)}$$

$$+\frac{G(\xi)\,[\mathrm{i}R_{\xi\xi}(\xi)+R^2(\xi)]}{2R_\xi^2(\xi)\,Z(\xi)}-\frac{G^*(\xi)}{Z(\xi)-\mathrm{e}^{-2h}/Z^*(\xi)}$$

$$+\sum_{\xi'=2}^{\xi'=n}\left[\frac{G^*(\xi')}{Z(\xi)-Z(\xi')}-\frac{G(\xi')}{Z(\xi)-\mathrm{e}^{-2h}/Z(\xi')}\right]=0. \tag{3.22}$$

These form a set of $2n$ equations, considering real and imaginary parts, as the imaginary parts for $\xi = 0$ and $\xi = n$ reduce to identities that can be easily checked in (3.12) taking into account that $Z(0)$ and $Z(n)$ are real.

There are $2n+2$ unknowns $x(\xi)$, $y(\xi)$ but $x(0) = 0$ and $x(n) = \pi$ are already chosen. Further unknowns are c, B and K; however these are catered for by equations (3.17), (3.18) and (3.19).

The resulting system of $2n+3$ nonlinear equations is solved by Newton iteration. The analytical form of the Jacobian has been found with the aid of the computer algebra program MACSYMA which also provides Fortran code.

The initial approximation is provided either by Tsao's (1959) third-order solution or by a previous solution. Iterations are stopped when residues are less than 10^{-10} which usually takes 4 to 7 iterations. The results are considered acceptable when the two sides of the relation

$$B=\tfrac{1}{2}c+\frac{1}{2\pi}\int_0^{2\pi}\tfrac{1}{2}u^2|_{y=-h}\,\mathrm{d}x-\zeta I/2\pi \tag{3.23}$$

where I is the excess impulse given below, agree to at least 5 decimal places. Computations are done on a Systime 8750 (equivalent to a VAX 11/750). To compute the second wave in figure 3(*b*), $h = 1$, $\zeta = 1$ and $H = 1$, correct to 5 decimal places, 11 points per half wave are enough. This result takes 6 iterations and 29.5 CPU seconds.

As well as checking against small-amplitude and irrotational results the calculations have been checked by an independent program for unsteady constant-vorticity waves which will be described in a future publication. The wave mentioned above, with $h = 1$, $\zeta = 1$ and $H = 1$, propagated for 50 periods. In that time the maximum slope changed 0.0006° and the height of the crest experienced a change of 0.000002, giving a good verification of both computations.

For the computation of limiting waves the program is modified by permitting an angle at the crest and taking one-sided difference formulae in which case equation (3.19) is replaced by

$$B-gy=0. \tag{3.24}$$

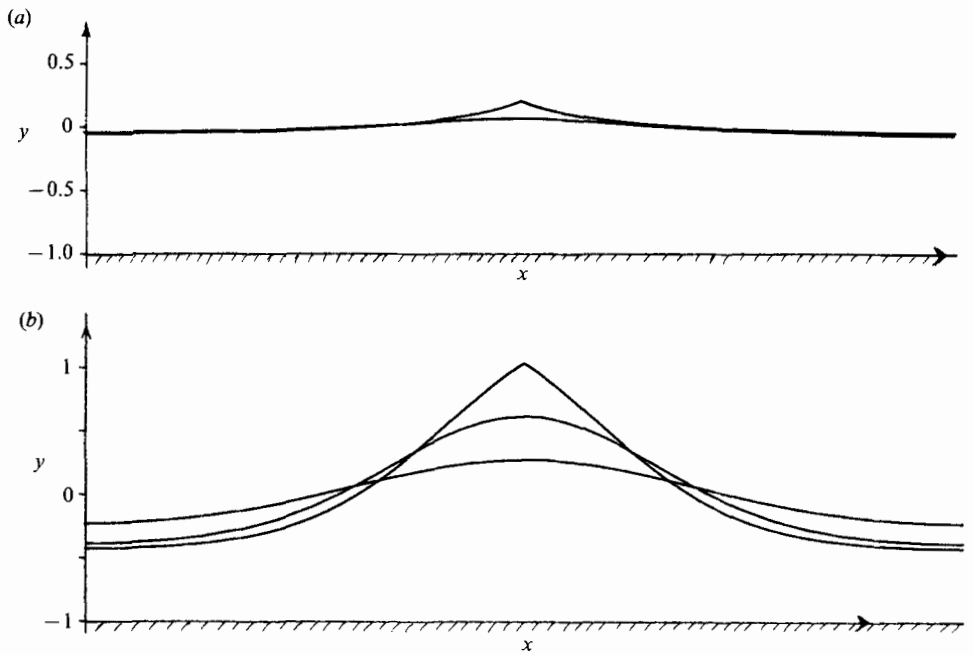

FIGURE 3. (*a*) Periodic waves with $\zeta = -1$ and $h = 1$: extreme wave with $H = 0.2549$, $c = 0.6280$; also $H = 0.12$, $c = 0.5883$. (*b*) Periodic waves with $\zeta = 1$ and $h = 1$: extreme wave with $H = 1.4589$, $c = 1.5408$; also $H = 1$, $c = 1.4421$; and $H = 0.5$, $c = 1.3580$.

Delachenal (1973) shows that the crest should have an angle of 120°, the vorticity only affects the curvature on each side. That result is assumed in the computations presented. When the angle is left free to be determined in the program, it is calculated to be within a fraction of a degree of 120°.

Integral quantities that are evaluated include the excess impulse

$$I = \int_0^{2\pi} \int_{-h}^{\eta} (\phi_x - \zeta y)\, \mathrm{d}y\, \mathrm{d}x + \int_0^{2\pi} \int_{-h}^{0} \zeta y\, \mathrm{d}y\, \mathrm{d}x, \tag{3.25}$$

excess kinetic energy:

$$2T = \int_0^{2\pi} \int_{-h}^{\eta} [(\phi_x - \zeta y^2) + \phi_y^2]\, \mathrm{d}y\, \mathrm{d}x - \int_0^{2\pi} \int_{-h}^{0} (\zeta y)^2\, \mathrm{d}y\, \mathrm{d}x, \tag{3.26}$$

excess potential energy:

$$2V = \int_0^{2\pi} g\eta^2\, \mathrm{d}x. \tag{3.27}$$

Applying Stokes's theorem to (3.25) and (3.26) we have

$$2T = \int_0^{2n} (cy - \tfrac{1}{2}\zeta y^2) \frac{\mathrm{d}\phi}{\mathrm{d}\xi}\, \mathrm{d}\xi + \tfrac{1}{3}\zeta^2 \int_0^{2n} \eta^3 \frac{\mathrm{d}x}{\mathrm{d}\xi}\, \mathrm{d}\xi, \tag{3.28}$$

$$I = \int_0^{2n} y \frac{\mathrm{d}\phi}{\mathrm{d}\xi} + \tfrac{1}{2}\zeta y^2 \frac{\mathrm{d}x}{\mathrm{d}\xi}\, \mathrm{d}\xi, \tag{3.29}$$

where the surface integrals are expressed in terms of the point parameter ξ.

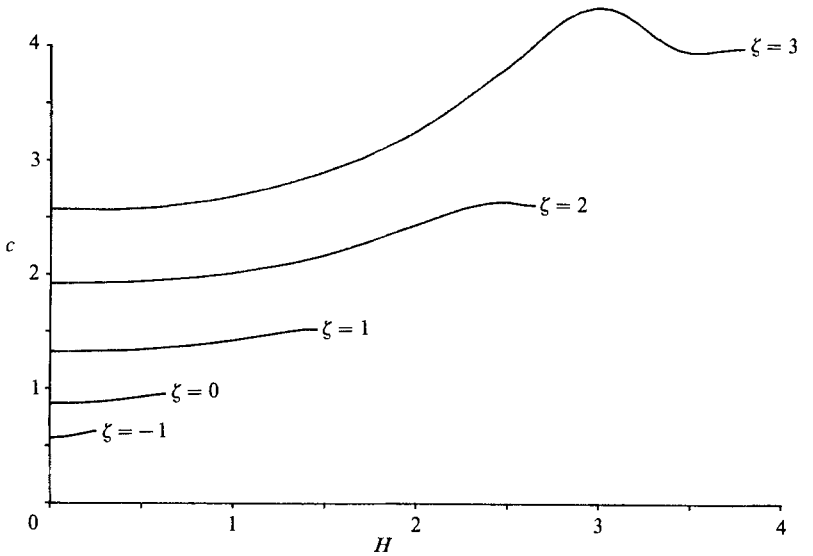

FIGURE 4. Graphs phase speed against wave height for five sets of periodic waves with $h = 1$: $\zeta = -1$, $\zeta = 0$, $\zeta = 1$, $\zeta = 2$, $\zeta = 3$.

4. Periodic waves

The solutions in our scaled variables have wavelength 2π and gravity unity, and depend on the three parameters: vorticity, ζ, wave height, H, and mean water depth h. Prominent characteristics of the effect of vorticity are already evident in Tsao's (1959) approximations and Simmen & Saffman's (1985) numerical solutions for deep water. For negative vorticity (waves propagating 'downstream') crests become sharper and smaller. For positive vorticity (waves propagating 'upstream') waves become more rounded, and for strong positive vorticity overhanging profiles and bizarre variations of phase velocity with height occur.

Our computations cover a region of the three-parameter space in which ζ varies from -1 to 3, h from 0.5 to 2 and H from zero to the extreme wave allowed by the other parameters. Representative examples are shown in figure 3, for $h = 1$ and $\zeta = \pm 1$. These figures, and all other figures showing wave profiles are without any vertical exaggeration. The effects of vorticity mentioned above are clear, as is the strong dependence on vorticity of the limiting wave height. The different curvatures at the crests of the limiting waves may also be noted. The phase velocities of waves for a wide range of vorticities for this depth of water are given in figure 4. As with irrotational waves velocity increases with amplitude except near the limiting waves. The variation with vorticity is mainly that which is evident in the linear dispersion equation (2.10). It is also clear that for larger vorticity very high waves with high speeds are possible. We discuss these waves below. One important feature where vorticity has a strong influence even on small amplitude waves is the partition of the energy density between kinetic energy, T, and potential energy V. For linear waves the ratio is

$$\frac{T}{V} = \frac{c_0^2}{c_1^2} = 1 + 2\lambda^2 + 2\lambda(1+\lambda^2)^{\frac{1}{2}}, \tag{4.1}$$

where

$$\lambda = \tfrac{1}{2}\zeta c_1^2/g = \tfrac{1}{2}\zeta(\tanh(kh))^{\frac{1}{2}}, \tag{4.2}$$

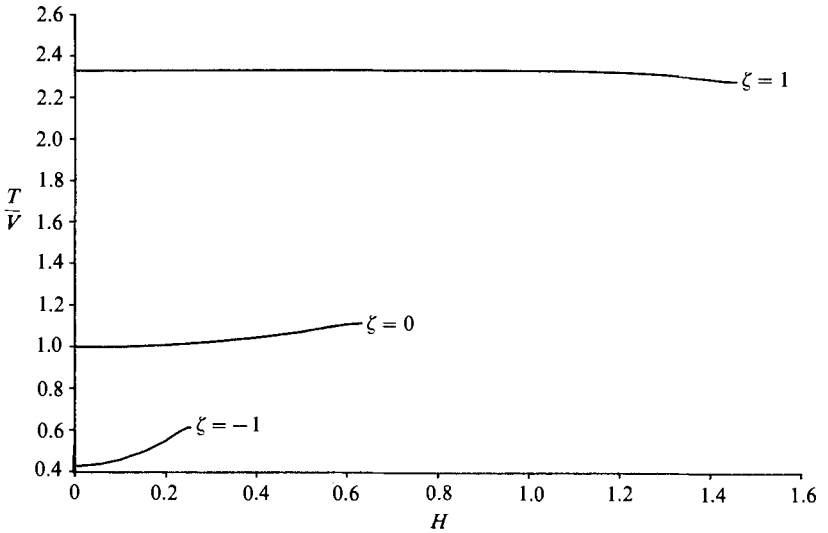

FIGURE 5. Graphs of T/V against wave height for three sets of periodic waves with $h = 1$: $\zeta = -1$, $\zeta = 0$ and $\zeta = 1$.

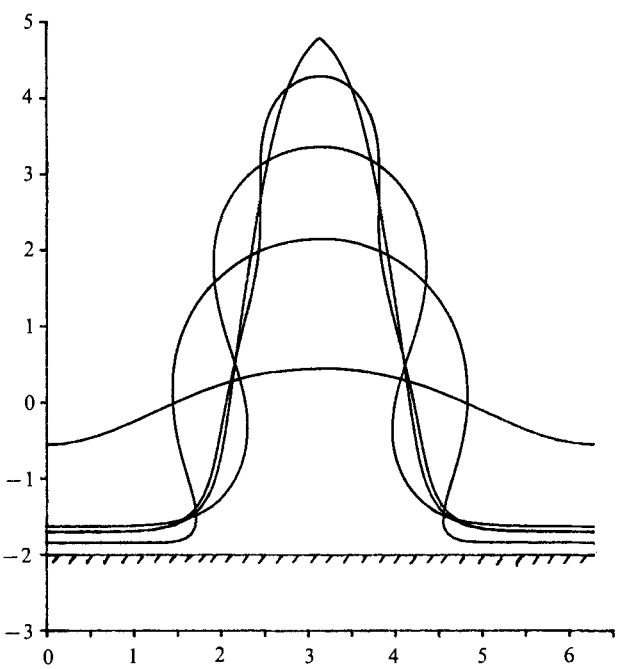

FIGURE 6. Periodic wave profiles for $h = 2$, $\zeta = 3$: extreme wave with $H = 6.489$, $c = 6.845$; also $H = 6$, $c = 6.748$; $H = 5$, $c = 7.110$; $H = 4$, $c = 6.906$; and $H = 1$, $c = 3.444$.

in dimensional units. Note that there is an appreciable variation of T/V in the range of vorticity $-1 \leqslant \zeta \leqslant 1$. The variation with wave amplitude for cases with $h = 1$ is shown in figure 5. This shows the importance of the linear ratio, relative to the amplitude variation. The substantial variation of the T/V ratio is not usually allowed for in the analysis of field and experimental wind waves. In such analysis linear irrotational flow results are normally used to calculate quantities such as

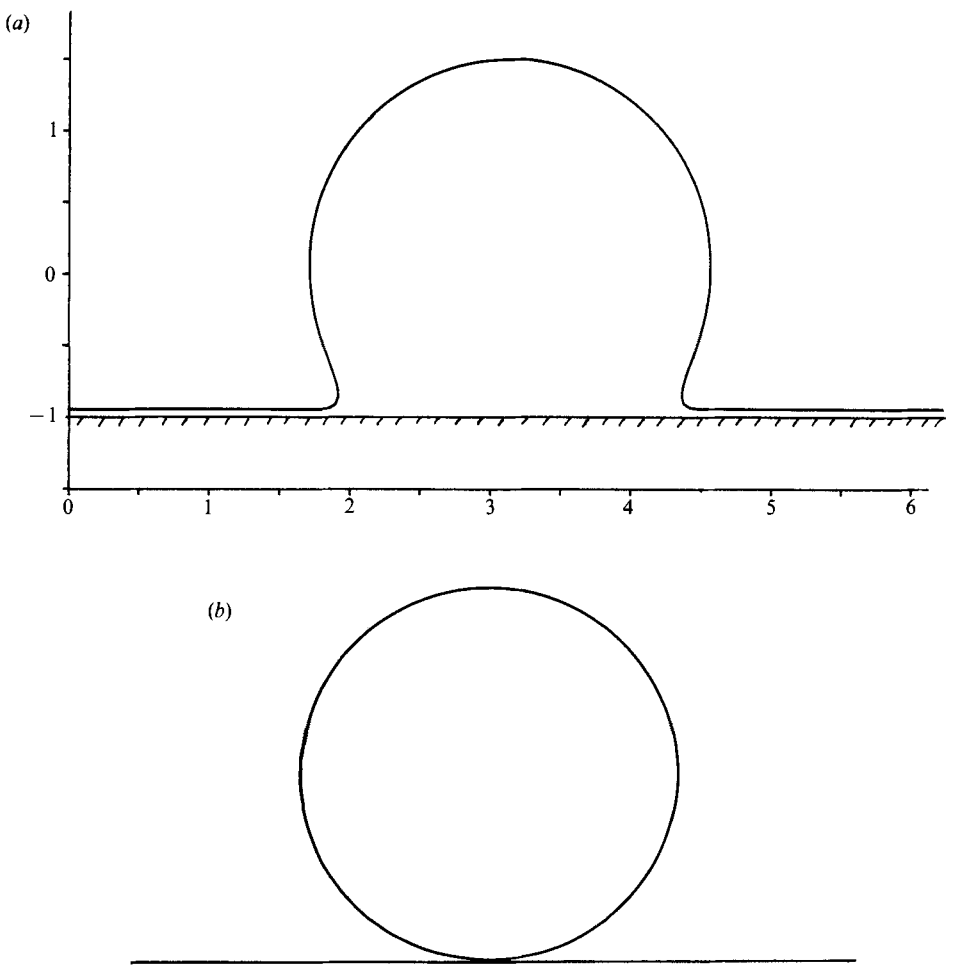

FIGURE 7. (*a*) Profile of a pure rotational wave ($g = 0$), with $\zeta = 1$, $H = 2.45$ and $c = 1.153$. (*b*) Sketch of a possible limiting wave, for zero gravity.

energy spectra from measurements of surface elevation. In strong winds the vorticity near the surface, may often be strong enough to make a suitable correction significant for the shorter waves. The dimensionless parameter λ defined in (4.2) shows that for waves of given wavenumber the effect of vorticity is less in shallow water, where the factor $\tanh(kh)$ is smaller than in deep water.

For values of vorticity larger than 1, Simmen & Saffman (1985) found waves with bizarre shapes and high phase velocities. Even stranger waves are found in finite water depths. A selection of wave profiles for $\zeta = 3$, $h = 2$, are shown in figure 6. For water of this depth surface waves are often treated as deep water waves since $\tanh(2) = 0.96$, however as figure 6 shows all the large waves have flat troughs which are clearly limited by the presence of the bed. Even for much greater values of h this phenomenon is evident.

It appears that the volume of water specified in a computation is the quantity most relevant in determining the range of large waves found. For finite depth of water the condition of zero mean level signifies a constant area $2\pi h$ in the

computation. Thus all the waves in figure 6 have the same volume of water above the bed. In deep water there is no volume constraint, nor is there such a constraint for solitary waves, unless volume above the mean surface level is used as a parameter to specify waves. The 'finite volume' also means that despite the existence of overhanging wave profiles, relatively large values of h are needed before it is possible for the overhangs to touch. Simmen & Saffman (1985, figure 9) have gaps in their solution branches due to touching and overlapping waves. By considering the following extreme case it is possible to estimate the volume of water required for an overlapping wave.

The large rounded waves have large values of vorticity, phase-velocity and of the ratio T/V. These suggest that vorticity and inertia are more important than gravity. It takes only a little imagination to move from the profiles of 'medium' height in figure 6 to a gravity-free wave which is shown in figure 7 (a). Further, the trend of solutions suggests that there may be a limiting wave which has a circular shape made up of water in rigid-body rotation as sketched in figure 7 (b). The fluid velocity is continuous with that in the layer of water beneath if the circle rolls on the surface. Clearly the thickness of the lower strip of water can have any value. If the circle were the limit of periodic waves then they would touch at a wavelength of 2π only if the mean level were greater than $\frac{1}{2}\pi^2$.

The circular vortex 'wave' can also be solitary. All the higher wave profiles in figure 6 have the character of solitary waves. That is, the troughs are flat and correspond to uniform sheared flow. Further features of these waves are discussed in the following section on solitary waves.

5. Solitary-wave solutions

The natural lengthscale for the study of solitary waves is the depth of the undisturbed flow, h, so that in presenting data, different units are now used with h and gravity as unity whereas for the periodic waves the wavelength is chosen as 2π. In particular, this means that values for vorticity are not directly comparable, for example the three highest waves with vorticity $\zeta = 3$ in figure 6 have vorticities $\Omega = 1.415$, $\Omega = 1.165$ and $\Omega = 1.283$ in order of increasing wave height, where Ω is the dimensionless vorticity in the new units. On the other hand infinitely many different periodic waves with flat troughs when scaled by the solitary-wave units based on water depth in the trough give the same solitary wave. That fact helps to clarify the interaction between vorticity and depth already mentioned for shallow-water periodic waves (see equations (4.1) and (4.2)). In these solitary wave units we denote the wave height by a. A different definition of wave velocity is also appropriate. We define S to be the wave velocity relative to the surface water in the region with constant depth, again taking figure 6 as an example, the three higher waves have $S = 4.162$, $S = 5.286$ and $S = 4.221$ in that order, whereas the values of c are $c = 2.008$, $c = 2.471$ and $c = 2.438$, respectively.

Most of the examples of solitary waves presented here were calculated by using the program for periodic waves with depth from trough to bed $h = 0.2$, that is with wavelength 10π times the depth, some with $h = 0.1$ and others with $h = 0.01$. An indication of accuracy is gained by comparison with irrotational wave results. The limiting irrotational solitary wave has height $a = 0.8332$ and velocity $S = 1.2909$ (Hunter & Vanden-Broeck 1983), whereas with 40 points per half wave we found 0.8302 and 1.2885 respectively. Profiles of the limiting irrotational solitary wave and the limiting waves for $\Omega = \pm 1$ are shown in figure 8. We have verified that the

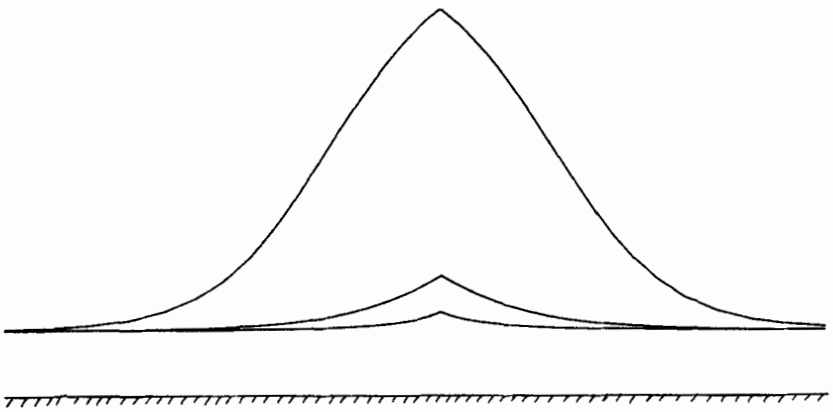

FIGURE 8. Profiles for the limiting solitary waves; for $\Omega = -1$, $a = 0.272$, $S = 0.738$; for $\Omega = 0$, $a = 0.830$, $S = 1.288$; and for $\Omega = 1$, $a = 4.898$, $S = 3.130$.

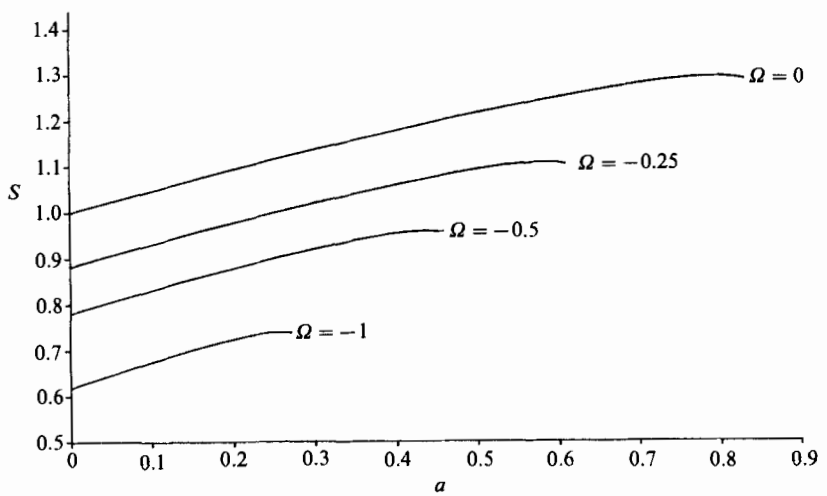

FIGURE 9. Graphs of solitary wave velocity against wave-height for four values of Ω: -1, -0.5, -0.25, 0.

periodic computations do permit appropriate exponential decay for the outskirts of these solitary waves.

The velocities S of a range of solitary waves are shown in figures 9 and 10. The approximate weakly nonlinear result of Benjamin (1962 equation (4.7)) is used for the low-amplitude results since these waves have a greater length than the limited region we use. The curves shown would lie much closer together if the velocity were taken relative to the mean flow, i.e. if $S - \frac{1}{2}\Omega$ were shown. Benjamin's result in our notation is

$$(S - \tfrac{1}{2}\Omega)^2 = 1 + \tfrac{1}{4}\Omega^2 + (1 + \tfrac{1}{3}\Omega^2)\, a + O(a^2). \tag{5.1}$$

The variations shown in figure 10 are more striking. Note the difference in scales between figures 9 and 10. The curves for $\Omega = 1.15$ and $\Omega = 1.175$ show that there may be as many as three different waves of the same height with different velocities. The 'loop' in the curve which grows rapidly with Ω once $\Omega > 1$ could not be fully defined for $\Omega = 1.2$. The limiting wave with a corner at its crest for $\Omega = 1.2$ has

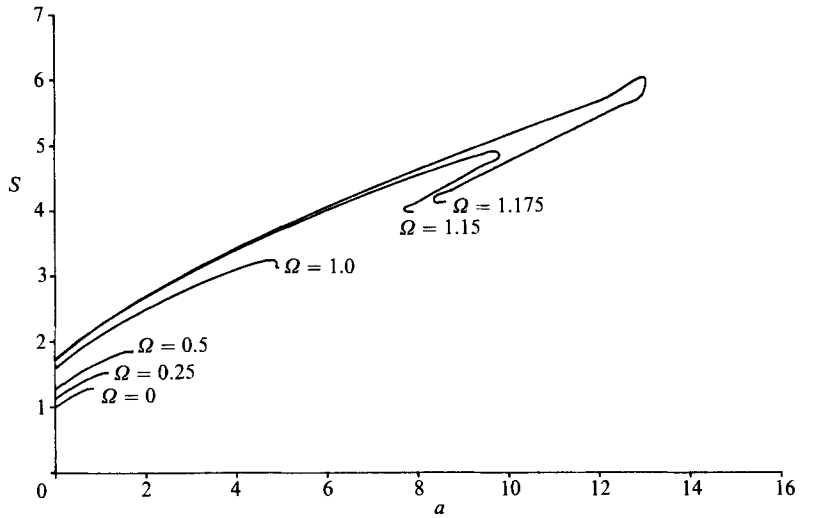

FIGURE 10. Graphs of solitary wave velocity against wave-height for six values of Ω: 0, 0.25, 0.5, 1.0, 1.15, 1.175.

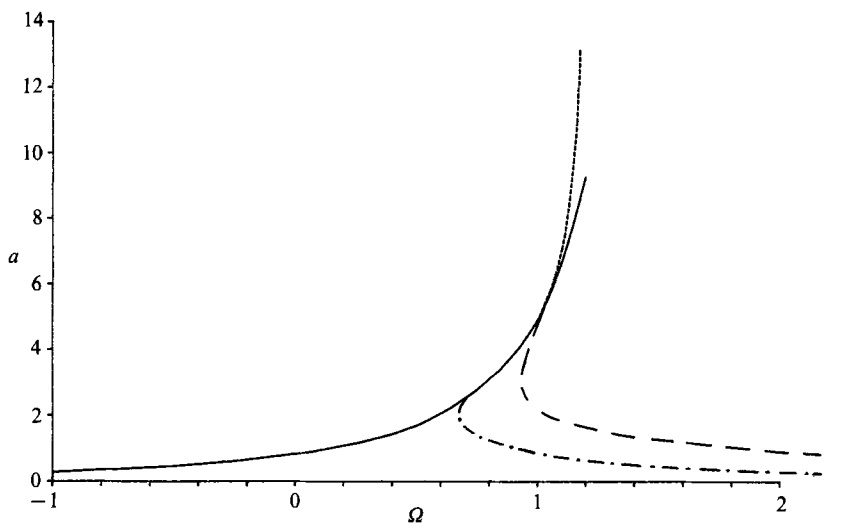

FIGURE 11. Curves in the vorticity, wave-height plane: ——, Extreme solitary waves; – – – –, Highest solitary waves; ——, Solitary waves with zero pressure gradients at their crests; ·····, Line separating solitary waves with eddies (above) from those without.

height $a = 9.28$, but the search for the highest wave on the two branches of the loop was stopped after waves of height approximately 34 and 40 were found. From the discussion at the end of the last section we expect the wave height and phase velocity of the higher and rounder waves can increase indefinitely for large enough vorticity.

In figure 11 we show four different curves: the first one gives the values for the wave-height of the limiting waves for values of Ω ranging from -1 to 1.175, we know that from $\Omega = -1$ to $\Omega = 1$ the limiting wave is the highest wave so, in that region, all the solutions stay between the horizontal axis (zero wave height) and the curve

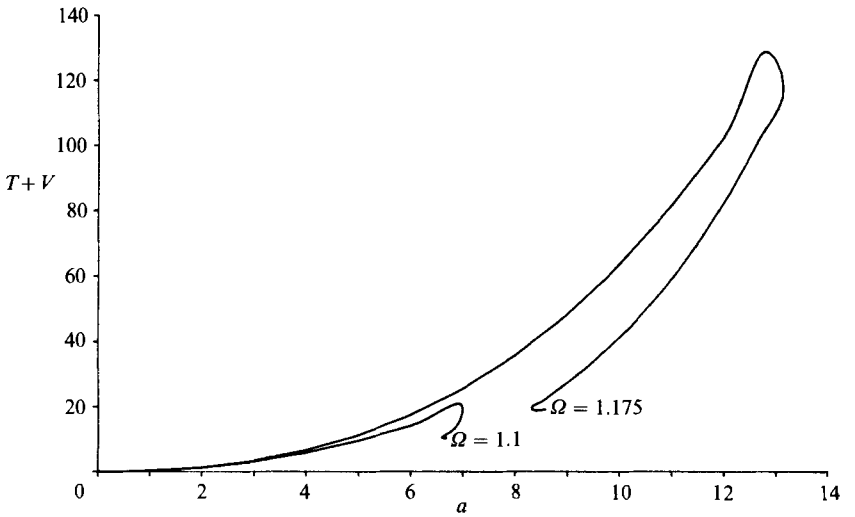

FIGURE 12. Graphs of total energy against wave height for solitary waves with $\Omega = 1.1$ and $\Omega = 1.175$.

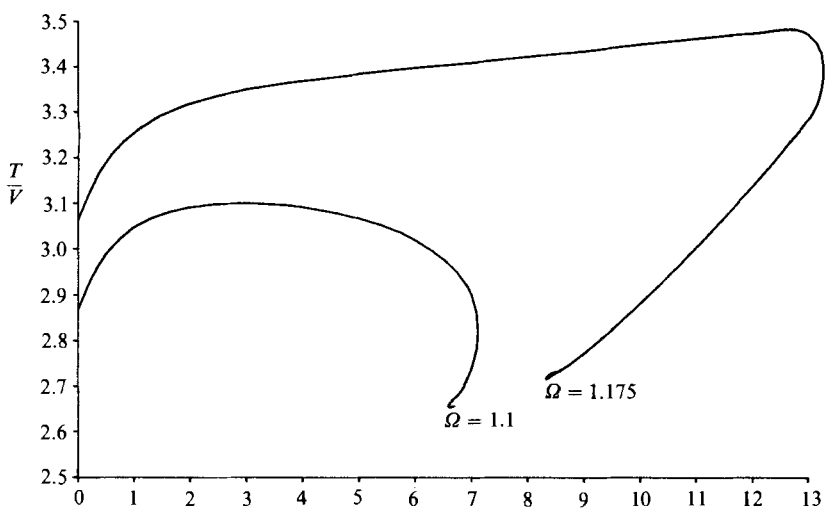

FIGURE 13. The ratio of kinetic energy to potential energy variation with wave height for solitary waves with $\Omega = 1.1$ and $\Omega = 1.175$.

of limiting waves, then for Ω slightly greater than 1 we start to have round waves higher than the limiting waves, the maximum values of a for those higher waves are shown by the curve that diverges from the curve of limiting waves, we could not compute many values since for values of $\Omega > 1.175$ they appear to increase extremely fast with Ω, as already noted. The third curve shows the boundary between waves with and without eddies beneath their crests. Eddies are discussed in the next section. Finally the last curve marks the divide between waves with the pressure underneath their crests below the atmospheric value and those with this pressure above that value, also discussed in the next section.

The values of energy both kinetic and potential for all the waves with $\Omega = 1.1$ and

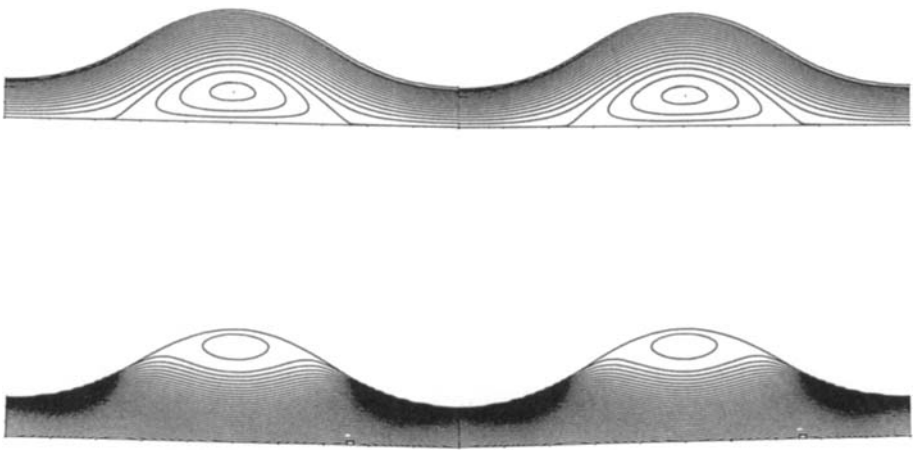

FIGURE 14. (*a*) Streamlines and (*b*) pressure contours for periodic wave with $\zeta = 2$, $h = 1$, $H = 1$. Rescaling in solitary wave units: $\Omega = 1.481$, $a = 1.823$ and $S = 3.302$ (not a good example of a solitary wave!).

$\Omega = 1.175$ are presented in figures 12 and 13. Figure 12 shows the values of total energy $(T + V)$ for both values of vorticity, and we find the same pattern as for wave speed; figure 13 shows the ratios T/V and we find again in a lesser scale the same behaviour. Considering the results in both figures we conclude that for high enough values of the vorticity Ω, as we increase wave height we move into a region of the solution space in which the waves have an excess of kinetic energy, over 80% of the total, and look very round in the manner of the pure vortical wave shown in the end of last section. Then as we proceed along the solution curve the share of kinetic energy is reduced in favour of potential energy. In other words we move from a region in which the vortical effects are dominant, the upper part of the folds, towards one in which gravity is more important, the lower portion of the folds. As vorticity increases there appears to be no bound for wave height and energy.

These results for solitary waves look closer to the results for deep-water waves presented by Simmen & Saffman (1985) than to those for periodic shallow-water waves, in the sense that the former show such peculiarities as folds in the curves for phase velocity against height and the existence of waves higher than extreme waves, that we did not find in the latter. Periodic deep-water waves and solitary waves have in common the infinite mass of available water unlike periodic shallow water waves. A solitary wave does not have the possibility of self interception so it cannot give rise to 'gaps' in the solution space.

6. Surface shear waves, eddies and stability

The large bulbous waves displayed in figures 3 and 11 can be better understood after examining the velocity and pressure fields beneath the surface. One representative wave is shown in figure 14. As may be seen there is a large closed eddy beneath the wave. Note also its velocity in solitary-wave units, $S = 3.302$, corresponds to a high Froude number. These large waves can be interpreted, if stationary, as a thin sheet of high-speed water passing over an eddy.

There is a close resemblance between these waves and the 'surface shear waves'

FIGURE 15. A surface shear wave occurring naturally in backwash on a beach.

described in Peregrine (1974). That model was stimulated by the observation of steep large rounded waves in the backwash of waves incident on beaches. Such a wave arising naturally is shown in the photograph of figure 15. Another surface shear wave also described in Peregrine (1974) is the 'wave hydraulic jump' (see also discussion of that paper). Both of these waves are easily reproduced in the laboratory, and are usually almost stationary on a fast moving stream. They occur over fixed beds, but also seem to have a counterpart in supercritical flow over antidunes on a mobile bed.

Peregrine's (1974) model does not depend on a specific vorticity distribution but simply characterizes the thin sheet of surface water by its momentum flux and considers its deflection due to hydrostatic pressure in the almost stagnant water beneath it. The ordinary differential equation so obtained for the shape of the wave is the same as that for the finite bending of a thin beam or elastica. This gives an easy way of comparing Peregrine's solution with the figures in this paper: just take a piece of paper or card and bend it whilst holding it at each side. Comparison with figure 14 will show that most of the wave closely follows such a curve.

The pressure field in figure 14(*b*) is easily interpreted in terms of a high-speed surface flow. A high transverse pressure gradient is required to turn the flow sharply at the base of the wave, hence the substantial excess pressures on the bed. Then over the main portion of the wave the pressure falls below atmospheric as in Peregrine's (1974) model, and 'sucks' the surface jet around in a curve which is tighter than the corresponding free-fall parabola. As the jet 'lands' near the bed once again high pressure gradients turn it back into a horizontal flow. To some extent the constant vorticity flow here may be a better model than Peregrine's for very steep waves over closed eddies. This is due to the Prandtl–Batchelor result that in two-dimensional high-Reynolds-number flow steady recirculating regions with closed streamlines have constant vorticity.

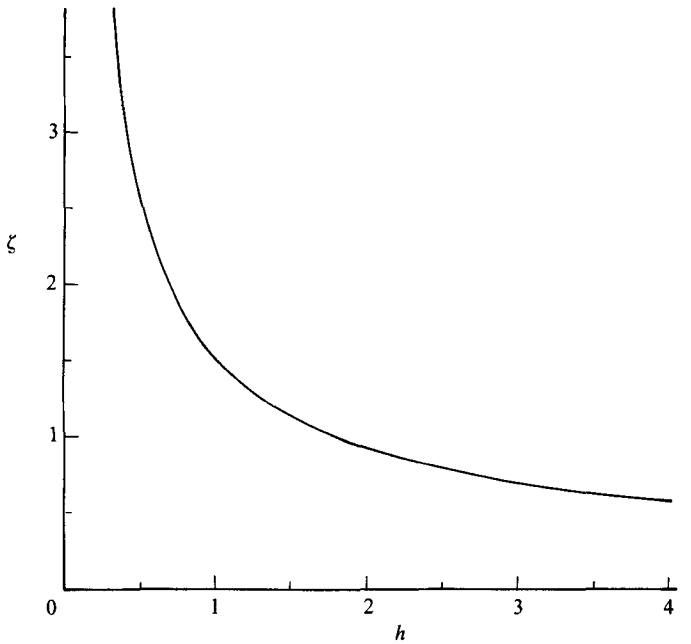

FIGURE 16. The boundary between waves with and without critical layers: linear theory.

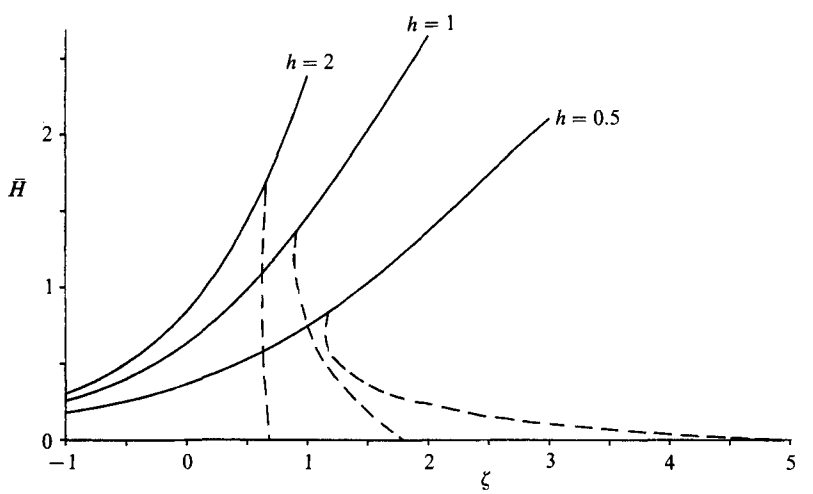

FIGURE 17. Vorticity and wave height for periodic waves, the full lines give the wave height of the limiting wave, for three different values of h, $h = 0.5$, 1 and 2, the broken lines mark the separation between waves with and without eddies for the corresponding depths.

Flow separation from a solid surface is often thought of as a viscous boundary-layer phenomenon. However, as these solutions show, separation to form an eddy occurs for inviscid flows with vorticity. This is not a new observation, Perry & Fairlie (1975) discuss an example where their inviscid model with vorticity gives streamlines for an eddy of separated flow which are similar to our free-surface example in figure 14(*a*).

Eddies also occur for the periodic waves. In fact if there is a critical layer above the bed 'cats eye' eddies form for any finite amplitude wave. Figure 16 shows the

FIGURE 18. Rear view of a naturally occurring surface shear wave in backwash. Note the way in which irregularities of the flow have grown as they pass over the crest of the wave.

boundary in the (ζ, h)-plane between linearized waves with and without a critical layer, given by (2.12). As already noticed the critical layer for infinitesimal waves is so deep that its influence on the waves is likely to be slight. Large waves are more likely to have eddies and figure 17 gives an indication of when this occurs.

The low pressure beneath the upper half of the wave means that the normal pressure gradient at the surface is opposite to the usual direction, with pressure lower than atmospheric in the water. This implies the surface is susceptible to Rayleigh–Taylor instability. This instability has its greatest growth rate for short wavelengths, but at the shortest scales surface tension is a stabilizing influence. In natural flows growth of the surface fluctuations due to initial turbulence is evident (see figure 18). The growth of small disturbances is limited by their translation through the unstable region thus waves on a laminar flow can be both smooth and steep. We also see such a growth of disturbances in unsteady computations.

7. Conclusions

We have presented some of the results of computations of steady periodic waves on a flow of uniform vorticity. In part these give results that are the expected extensions of the approximate-Stokes wave type of expansion of Tsao (1959), the stream-function approximation of Dalrymple (1974) and the deep-water results obtained by Simmen & Saffman (1985) using a similar numerical method. Since these results lack novelty, and precise numerical results are not of direct value for applications because of the special vorticity distribution, we have given only a short account of the periodic waves.

However it should be noted that there is a large variation in the ratio of kinetic energy to potential energy. This implies that conventional measurements of wind waves which use only surface elevation may give a poor approximation to the total wave energy when there are steep waves riding on a significant wind drift current.

The solitary waves with positive vorticity, that is with vorticity such as a wave propagating against a stream would meet, show striking effects with large bulbous waves which have no apparent upper limit on their size. There are parallels with the stationary 'surface shear waves' described by Peregrine (1974). We consider that the character of the bulbous waves is independent of the precise nature of their vorticity distribution and the solutions presented here are likely to be a better model than Peregrine's very simple stationary shear layer. Solutions of this type are also described by Pullin & Grimshaw (1988).

Surface shear waves arise readily as stationary waves on high-Froude-number flows. We note that the upper portion of such waves has a pressure in the water that is less that atmospheric. This permits growth of Rayleigh–Taylor instabilities which are evident when the waves form on turbulent flows.

An aspect of wider interest in fluid dynamics is the flow separation that occurs from the bed in the steep waves. A closed eddy occurs for the upstream propagating waves whenever there is a critical layer in the flow. However, the critical layer for infinitesimal waves is always at a depth where wave induced flow is small and the cats-eye eddies, which we obtain (and do not document here) are not important for the surface flow (see also Peregrine 1976, §14, B3). For the solitary waves eddies are important. Figure 11 gives an indication of the region in parameter space in which eddies occur. We would particularly like to note that in unsteady flows, such as the backwash on beaches, the surface shear waves arise spontaneously and slowly evolve in shape. Any slowly varying type of solution is very likely to follow a trajectory in parameter space which crosses the boundary between waves without eddies to waves with eddies. Such a transition involves a flow separation from the bed which may be entirely inviscid in character.

A. F. T. da S. acknowledges financial support from 'Conselho Nacional de Pesquisas e Desenvolvimento Tecnólogico' Cnpq, grant reference number 20.2554/85-MA.

REFERENCES

Banner, M. L. & Phillips, O. M. 1974 On the incipient breaking of small scale waves. *J. Fluid Mech.* **65**, 647–656.

Benjamin, T. B. 1962 The solitary wave on a stream with an arbitrary distribution of vorticity. *J. Fluid Mech.* **12**, 97–116.

Caulliez, G. 1987 Structure des mouvements associés aux vagues de capilarité-gravité générées par le vent. PhD thesis, l'Université de d'Aix-Marseille II.

Dalrymple, R. A. 1974 A finite amplitude wave on a linear shear current. *J. Geophys. Res.* **79**, 4498–4504.

Delachenal, M. B. 1973 Existence d'écoulement permanent de type coin pour un fluide parfait a surface libre. *C. R. Acad. Sci. Paris* A **276**, 1021–1024.

Dold, J. W. & Peregrine, D. H. 1986 An efficient boundary-integral method for steep unsteady water waves. In *Numerical methods for Fluid Dynamics* vol. 2 (ed. K. W. Morton & M. J. Baines), pp. 671–679. Clarendon Press.

Hunter, J. K. & Vanden-Broeck, J. M. 1983 Accurate computations for steep solitary waves. *J. Fluid Mech.* **136**. 63–71.

Peregrine, D. H. 1974 Surface shear waves. *J. Hydraul. Div. ASCE* **100**, 1215–1227. [Discussion in **101**, 1032–1034 (1975).]

Peregrine, D. H. 1976 Interaction of water waves and currents. *Adv. Appl. Mech.* **16**, 9–117.

Perry A. & Fairlie, B. D. 1975 A study of turbulent boundary-layer separation and reattachment. *J. Fluid Mech.* **69**, 657–672.

PHILLIPS, O. M. & BANNER, M. L. 1974 Wave breaking in the presence of wind drift and swell. *J. Fluid Mech.* **66**, 625–640.

PULLIN, D. I. & GRIMSHAW, R. H. 1985 Interfacial progressive gravity waves in a two layer shear flow. *Phys. Fluids* **26**, 1731–1739.

PULLIN, D. I. & GRIMSHAW, R. H. 1988 Finite amplitude solitary waves at the interface between two homogeneous fluids. Submitted for publication.

SIMMEN, J. A. & SAFFMAN, P. G. 1985 Steady deep water waves on a linear shear current. *Stud. Appl. Maths* **73**, 35–57.

STOKES, G. G. 1847 On the theory of oscillatory waves. *Trans. Camb. Phil. Soc.* **8**, 441–455.

TANAKA, M. 1983 The stability of steep gravity waves. *J. Phys. Soc. Japan* **52**, 3047–3055.

TANAKA, M. 1985 The stability of steep gravity waves. Part 2. *J. Fluid Mech.* **156**, 281–289.

TSAO, S. 1959 Behaviour of surface waves on a linearly varying current. *Tr. Mosk. Fiz.-Tekh. Inst. Issled. Mekh.*